Free-space terahertz radiation from a LT-GaAs-on-quartz large-area photoconductive emitter

DAVID R. BACON,[1,*] ANDREW D. BURNETT,[1,2] MATTHEW SWITHENBANK,[1] CHRISTOPHER RUSSELL,[1] LIANHE LI,[1] CHRISTOPHER D. WOOD,[1] JOHN CUNNINGHAM,[1] EDMUND H. LINFIELD,[1] A. GILES DAVIES,[1] PAUL DEAN,[1] AND JOSHUA R. FREEMAN[1,3]

[1] School of Electronic and Electrical Engineering, University of Leeds, Woodhouse Lane, Leeds LS9 2JT, UK
[2] School of Chemistry, University of Leeds, Woodhouse Lane, Leeds LS9 2JT, UK
[3] j.r.freeman@leeds.ac.uk
[*] el09d2b@leeds.ac.uk

Abstract: We report on large-area photoconductive terahertz (THz) emitters with a low-temperature-grown GaAs (LT-GaAs) active layer fabricated on quartz substrates using a lift-off transfer process. These devices are compared to the same LT-GaAs emitters when fabricated on the growth substrate. We find that the transferred devices show higher optical-to-THz conversion efficiencies and significantly larger breakdown fields, which we attribute to reduced parasitic current in the substrate. Through these improvements, we demonstrate a factor of ~8 increase in emitted THz field strength at the maximum operating voltage. In addition we find improved performance when these devices are used for photoconductive detection, which we explain through a combination of reduced parasitic substrate currents and reduced space-charge build-up in the device.

References and links

1. D. Auston, A. Johnson, P. Smith, and J. Bean, "Picosecond optoelectronic detection, sampling, and correlation measurements in amorphous semiconductors," Appl. Phys. Lett. **37**, 371–373 (1980).
2. Y. Shen, P. Upadhya, H. Beere, E. Linfield, A. Davies, I. Gregory, C. Baker, W. Tribe, and M. Evans, "Generation and detection of ultrabroadband terahertz radiation using photoconductive emitters and receivers," Appl. Phys. Lett. **85**, 164–166 (2004).
3. A. Warren, N. Katzenellenbogen, D. Grischkowsky, J. Woodall, M. Melloch, and N. Otsuka, "Subpicosecond, freely propagating electromagnetic pulse generation and detection using GaAs: As epilayers," Appl. Phys. Lett. **58**, 1512–1514 (1991).
4. M. Tani, K.-S. Lee, and X.-C. Zhang, "Detection of terahertz radiation with low-temperature-grown GaAs-based photoconductive antenna using 1.55 μm probe," Appl. Phys. Lett. **77**, 1396–1398 (2000).
5. A. G. Davies, A. D. Burnett, W. Fan, E. H. Linfield, and J. E. Cunningham, "Terahertz spectroscopy of explosives and drugs," Mater. Today **11**, 18–26 (2008).
6. B. M. Fischer, H. Helm, and P. U. Jepsen, "Chemical recognition with broadband THz spectroscopy," Proc. IEEE **95**, 1592–1604 (2007).
7. M. Brucherseifer, M. Nagel, P. H. Bolivar, H. Kurz, A. Bosserhoff, and R. Büttner, "Label-free probing of the binding state of DNA by time-domain terahertz sensing," Appl. Phys. Lett. **77**, 4049–4051 (2000).
8. K. Peiponen, A. Zeitler, and M. Kuwata-Gonokami, eds., *Terahertz Spectroscopy: Theory and Applications* (Springer, 2012).
9. G. Segschneider, T. Dekorsy, H. Kurz, R. Hey, and K. Ploog, "Energy resolved ultrafast relaxation dynamics close to the band edge of low-temperature grown GaAs," Appl. Phys. Lett. **71**, 2779–2781 (1997).

10. S. Gupta, J. F. Whitaker, and G. Mourou, "Ultrafast carrier dynamics in iii-v semiconductors grown by molecular-beam epitaxy at very low substrate temperatures," Quantum Electron. IEEE J. **28**, 2464–2472 (1992).
11. M. Tani, S. Matsuura, K. Sakai, and S.-i. Nakashima, "Emission characteristics of photoconductive antennas based on low-temperature-grown GaAs and semi-insulating GaAs," Appl. Opt. **36**, 7853–7859 (1997).
12. M. Tani, K. Sakai, and H. Mimura, "Ultrafast photoconductive detectors based on semi-insulating GaAs and InP," Jpn. J. Appl. Phys. **36**, L1175 (1997).
13. C. Russell, C. D. Wood, A. D. Burnett, L. Li, E. H. Linfield, A. G. Davies, and J. E. Cunningham, "Spectroscopy of polycrystalline materials using thinned-substrate planar goubau line at cryogenic temperatures," Lab on a Chip **13**, 4065–4070 (2013).
14. J. Cunningham, C. Wood, A. Davies, I. Hunter, E. Linfield, and H. Beere, "Terahertz frequency range band-stop filters," Appl. Phys. Lett. **86**, 213503 (2005).
15. H.-M. Heiliger, M. Vossebürger, H. Roskos, H. Kurz, R. Hey, and K. Ploog, "Application of liftoff low-temperature-grown GaAs on transparent substrates for THz signal generation," Appl. Phys. Lett. **69**, 2903–2905 (1996).
16. M. Awad, M. Nagel, H. Kurz, J. Herfort, and K. Ploog, "Characterization of low temperature GaAs antenna array terahertz emitters," Appl. Phys. Lett. **91**, 181124 (2007).
17. R. D. V. Ríos, S. Bikorimana, M. A. Ummy, R. Dorsinville, and S.-W. Seo, "A bow-tie photoconductive antenna using a low-temperature-grown GaAs thin-film on a silicon substrate for terahertz wave generation and detection," J. Opt. **17**, 125802 (2015).
18. X. Zheng, Y. Xu, R. Sobolewski, R. Adam, M. Mikulics, M. Siegel, and P. Kordoš, "Femtosecond response of a free-standing LT-GaAs photoconductive switch," Appl. optics **42**, 1726–1731 (2003).
19. A. Halpern, *Schaum's Outline Beginning Physics II* (McGraw-Hill Companies Inc, 1998).
20. L. Hou and W. Shi, "An LT-GaAs terahertz photoconductive antenna with high emission power, low noise, and good stability," Electron Devices, IEEE Transactions on **60**, 1619–1624 (2013).
21. M. Naftaly and R. E. Miles, "Terahertz time-domain spectroscopy for material characterization," Proceedings-IEEE **95**, 1658 (2007).
22. D. Grischkowsky, S. Keiding, M. Van Exter, and C. Fattinger, "Far-infrared time-domain spectroscopy with terahertz beams of dielectrics and semiconductors," JOSA B **7**, 2006–2015 (1990).
23. J. Luo, H. Thomas, D. Morgan, D. Westwood, and R. Williams, "The electrical breakdown properties of GaAs layers grown by molecular beam epitaxy at low temperature," Semicond. Sci. Technol. **9**, 2199 (1994).
24. E. Yablonovitch, D. Hwang, T. Gmitter, L. Florez, and J. Harbison, "Van der waals bonding of GaAs epitaxial liftoff films onto arbitrary substrates," Appl. Phys. Lett. **56**, 2419–2421 (1990).
25. Y. Shen, P. Upadhya, E. Linfield, H. Beere, and A. Davies, "Ultrabroadband terahertz radiation from low-temperature-grown GaAs photoconductive emitters," Appl. Phys. Lett. **83**, 3117–3119 (2003).
26. Q. Wu and X.-C. Zhang, "Free-space electro-optic sampling of terahertz beams," Appl. Phys. Lett. **67**, 3523–3525 (1995).
27. Y.-S. Lee, *Principles of Terahertz Science and Technology*, vol. 170 (Springer Science & Business Media, 2009).
28. B. Hu, X.-C. Zhang, and D. Auston, "Temperature dependence of femtosecond electromagnetic radiation from semiconductor surfaces," Appl. Phys. Lett. **57**, 2629–2631 (1990).
29. D. Aspnes and A. Studna, "Dielectric functions and optical parameters of Si, Ge, GaP, GaAs, GaSb, InP, InAs, and InSb from 1.5 to 6.0 ev," Phys. Rev. B **27**, 985 (1983).
30. M. V. Fischetti, "Monte carlo simulation of transport in technologically significant semiconductors of the diamond and zinc-blende structures. i. homogeneous transport," IEEE Transactions on Electron Devices **38**, 634–649 (1991).
31. M. Wellner, *Elements of Physics* (Springer Science & Business Media, 2012).
32. R. Carlson, G. Slack, and S. Silverman, "Thermal conductivity of GaAs and GaAs1- xpx laser semiconductors," J. Appl. Phys. **36**, 505–507 (1965).
33. J. Blakemore, "Semiconducting and other major properties of gallium arsenide," J. Appl. Phys. **53**, R123–R181 (1982).
34. F. Sizov and A. Rogalski, "THz detectors," Prog. Quantum Electron. **34**, 278–347 (2010).
35. P. U. Jepsen, R. H. Jacobsen, and S. Keiding, "Generation and detection of terahertz pulses from biased semiconductor antennas," JOSA B **13**, 2424–2436 (1996).
36. L. Wang, Y. Liu, Y. Wang, and Z. Zhao, "A method for removing echoes in the terahertz time-domain spectroscopy system," in "Microwave and Millimeter Wave Technology (ICMMT), 2012 International Conference on," vol. 2 (IEEE, 2012), vol. 2, pp. 1–4.
37. O. Hirsch, P. Alexander, and L. F. Gladden, "Techniques for cancellation of interfering multiple reflections in terahertz time-domain measurements," Microelectron. J. **39**, 841–848 (2008).
38. M. Naftaly and R. Miles, "A method for removing etalon oscillations from THz time-domain spectra," Opt. Commun. **280**, 291–295 (2007).

1. Introduction

Photoconductive (PC) switches [1], triggered by femtosecond lasers are widely used for both the generation and detection of free-space terahertz (THz) radiation [2–4]. Much progress has

been made on the development of these devices in recent years, resulting in the realisation of photoconductive switches with sub-picosecond switching times in several material systems. This has led to their widespread use in terahertz time-domain spectroscopy (THz-TDS) leading to several commercial applications of THz-TDS, including the detection of explosives [5], identification of biochemicals [6, 7], and non-destructive testing [8]. Nevertheless, the use of PC switches for time-domain spectroscopy requires devices that can provide high signal-to-noise ratios needed to measure a range of samples, and the systems should also exhibit a high frequency resolution to allow the distinction of narrow spectral features.

For PC THz emission, a femtosecond optical laser pulse with energy greater than the semi-conductor bandgap is focused onto the PC material between a pair of biased electrodes, causing generation and acceleration of electron-hole pairs. This transient current gives rise to a single cycle electromagnetic pulse, with a spectrum typically covering the 0.1–5 THz range—the THz signal is proportional to the derivative of the transient photo-current. The THz power and band-width available from a PC emitter are dependent on several fundamental material-dependent parameters including the carrier lifetime, mobility, dark resistivity and breakdown voltage. A well-suited material will have a short carrier lifetime to ensure the transient photo-current is short, a high mobility to ensure a large photo-current, a high dark resistivity to minimise excess heating from the applied bias, and a large breakdown voltage so that a high bias can be applied to maximise photo-current. When used in detection, the carriers are instead accelerated by an incident THz field, after being generated by an optical pulse. In this case the detected photo-current is proportional to the incident THz field. For detection, a good material will possess a very short carrier lifetime and high mobility, but breakdown voltage and dark resistivity are less important since no DC bias is applied.

When exciting at 800 nm, the best-performing material for PC switches is low-temperature-grown gallium arsenide (LT-GaAs) which incorporates excess arsenic trapping sites to ensure a very short carrier lifetime, typically ~300 fs [9, 10]. It also exhibits very high breakdown fields ($500\,\mathrm{kV\,cm^{-1}}$) [11], relatively good mobility and high dark resistance, compared with semi-insulating (SI)-GaAs or silicon-on-sapphire [3]. The short carrier lifetime also makes it an ideal material for PC detection [12]. LT-GaAs is typically fabricated by single crystal growth, either directly on a SI-GaAs wafer or separated by a thin insulating layer of AlAs. Electrodes are then fabricated directly on the LT-GaAs surface to form an LT-GaAs emitter/detector on an SI-GaAs substrate.

In this work, we demonstrate high power free-space emission and sensitive detection of THz radiation using LT-GaAs transferred onto quartz substrates, a technique that has proven successful in on-chip THz waveguides [13, 14]. To date, three examples of free-space THz radiation emission have been demonstrated using LT-GaAs bonded with sapphire [15–17], as well as one instance of LT-GaAs bonded with Si and MgO for on-chip applications [18]. However, these did not provide a comprehensive comparison between lift-off-transfer (LOT) devices and devices fabricated 'as-grown' on the SI-GaAs substrate, the latter of which are very widely used. Furthermore, the devices were fabricated with relatively small gap sizes compared with those demonstrated here, in order to produce high applied fields at low bias voltages.

In this work, Z-cut quartz has been chosen as a substrate as it possesses a significantly higher electrical resistivity [19], when compared with SI-GaAs [20]. It also exhibits low losses in the THz region, and is transparent to 800 nm light. Its low refractive index in the THz region of approximately 1.9 [21], compared to 3.6 in SI-GaAs [22], can also be a useful attribute in THz-TDS systems. To demonstrate these advantages of using Z-cut quartz, we make use of two separate collection techniques shown in Fig. 1. The first is a THz transmission geometry, in which optical excitation and THz collection occur on opposite sides of the device; the advantage of a low-index substrate here is that a smaller percentage of the THz pulse is reflected back into the substrate at the substrate-air interface, in comparison to when using SI-GaAs. In

transmission, this problem can also be solved by incorporating a hyper-hemispherical silicon lens, which is well index-matched to SI-GaAs. In reflection geometry, however, excitation and collection occur on the same side of the device. In this orientation, a higher percentage of the generated signal should be emitted from the excited side, when compared with a device mounted on SI-GaAs. We show that our devices provide higher optical-to-THz conversion efficiencies and significantly larger breakdown fields when compared to SI-GaAs devices, which we attribute to reduced parasitic current in the substrate. In addition we find improved performance when these devices are used for photoconductive detection, which we explain through a combination of reduced parasitic substrate currents and reduced space-charge build-up in the device.

2. Fabrication

Three device types were fabricated: LT-GaAs devices on an SI-GaAs substrate (LoG); LT-GaAs devices on a quartz substrate (LoQ), and bulk SI-GaAs. The initial fabrication steps for the LT-GaAs devices are independent of the eventual substrate. A 2-μm-thick layer of LT-GaAs was grown at 210 °C, using molecular beam epitaxy, on a 100-nm-thick sacrificial AlAs layer, itself grown on a 500-μm-thick SI-GaAs wafer. After the wafer was scribed and diced, each piece was placed into a rapid thermal annealer for 15 minutes at 575 °C to increase the resistivity [23]. The procedure for the quartz device was similar to that described by Cunningham *et al*. in [14]. For transfer to quartz, protective wax (Wax W, Apiezon) was melted (~100 °C) onto the surface of the LT-GaAs, before it was placed in a sulphuric etch solution (H_2SO_4:H_2O_2:H_2O, 1:40:80 by vol) for 1 minute to expose the AlAs layer. The samples were then placed in a dilute HF solution (HF:H_2O, 1:9) for 24 hours at 4 °C to remove the AlAs layer. Once released, the 2-μm-thick LT-GaAs layer, supported by the wax, was transferred onto a clean Z-cut-quartz substrate, the thickness of which was dependent on the intended experimental collection geometry. However, unless otherwise stated a 2-mm-thick quartz substrate was used. The samples were then left for ~1 week for van der Waals [24] bonding to occur. The wax was then removed using trichloroethylene and the samples were placed in a vacuum oven (20 m) for 15 hours at 250 °C, to remove any excess moisture and aid adhesion. Metal electrodes (Ti:Au, 10:150 nm) were then defined on all devices using standard lithographic techniques and thermal evaporation. We note here that for the LoQ device, the gold contacts overlay the LT-GaAs and the quartz. Therefore the initial sample size used for fabrication is limited only by the desired gap width of the antenna. However, this is not the case for the LoG device, since the LT-GaAs layer is supported by the SI-GaAs substrate. Consequently, the sample size of the LoG device is limited by the size of the electrical contacts and the device mounting technique used in the experimental setup. The fabrication process for a LoQ device, therefore, proves to be significantly more efficient in its use of LT-GaAs. The LT-GaAs thickness of 2-μm was chosen for this study because the growth conditions for this thickness have been optimised.

3. Experimental characterization of emitters and detectors

For this work, a large-area slot electrode design with a 200-μm-wide and 4-mm-long gap was used. Each device was mounted onto a pre-designed printed circuit board using conductive silver paint. For initial measurements, devices were positioned in a THz-TDS system similar to that described by Shen *et al*. in [25]. All emitters were electrically biased with a modulation frequency of 7 kHz, with a 50 % duty cycle, to enable lock-in detection of the detected signal. The system was driven by a 800 nm wavelength mode-locked Ti:sapphire laser (Vitara, Coherent) providing pulses with a width of 20 fs at an 80 MHz repetition rate. The optical beam was split into two parts, the more powerful of which (the 'pump') was focused down to a circular spot on the surface of the emitter through an off-axis parabolic mirror, which was then used to collect

and collimate the THz radiation generated. In reflection geometry, the THz radiation from the emitter was collected from the laser excited surface, eliminating losses and dispersion from the substrate and resulting in higher bandwidths. In the transmission geometry, radiation was collected from the substrate side. The collected radiation was then focused onto a detector using a second parabolic mirror, along with the weaker 'probe' beam with average optical power up to 120 mW. A delay stage was used to vary the arrival time between the THz pulse and probe pulse on the detector. Two detection methods were used in this work, the first being electro-optic (EO) sampling [26] using a 150 µm-thick GaP crystal paired with balanced photodiodes. The THz field incident on the EO crystal was calculated using an expression presented in [27]. The second method used a photoconductive switch, identical to those used for THz generation. The current generated in the photoconductive switch was amplified using a transimpedance amplifier with a gain of 1×10^8 Ω. For both techniques, the signal was recorded using a lock-in amplifier, referenced to the emitter bias-modulation frequency. All data shown was collected in a nitrogen environment to remove the effect of water absorption in atmosphere.
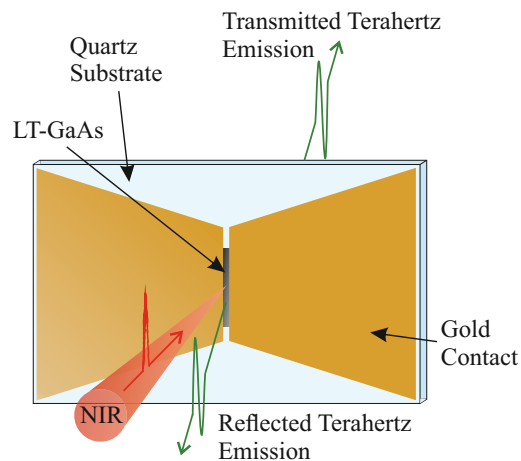

Fig. 1. A photoconductive device generating terahertz radiation in reflection (towards reader) and transmission (away from reader) geometries.

4. Results and discussion

4.1. Emission

Table 1. Typical values of resistance for the three types of devices discussed in the text. The values have been extracted from fitting IV curves for each device. Conditions 'light' (and 'dark') refer to the presence (absence) of an optical beam (20 mW average power), focused onto the emitter and aligned to minimise resistance.

Condition	Device Type		
	LT-GaAs-on-SI-GaAs (LoG)	LT-GaAs-on-quartz (LoQ)	Bulk SI-GaAs
Light	17.5 MΩ	74.9 MΩ	8.5 kΩ
Dark	33.5 MΩ	5.3 GΩ	31.0 MΩ

The typical resistance values for LoG, LoQ and bulk SI-GaAs emitters were obtained from current-voltage (I-V) measurements, and are summarised in Table 1 for both light (average

incident power 20 mW) and dark conditions. For THz emission, the principal benefit of a high resistance is that current induced heating in the device is reduced; heating is known to have a detrimental effect on the carrier mobility and efficiency of SI-GaAs photoconductive emitters [28]. A high dark resistance allows higher bias to be applied and therefore greater output powers can be obtained [15]. A comparison between the devices shows that the LoQ devices exhibit a dark resistance approximately two orders of magnitude greater than those on SI-GaAs. We attribute this greater value to the absence of an additional current path through the SI-GaAs substrate and the reduced area of LT-GaAs used in fabrication. The LoQ device also shows a higher resistance under illumination. This difference can be accounted for by considering transmission through the LT-GaAs layer. For 2-μm-thick LT-GaAs used here, we calculate that ~5 % of the incident optical beam is transmitted into the SI-GaAs substrate. For this calculation, an absorption coefficient at 800 nm of $1.3\,\mu m^{-1}$ [29] was assumed, and the interface reflections were taken into account. The thin layer of AlAs was deemed to have a negligible effect on the transmission of the optical beam, since it possesses a large bandgap of 2.13 eV relative to the LT-GaAs [30]. Despite only 5 % of the incident optical beam generating electron-hole pairs in the SI-GaAs substrate, this clearly has a significant influence on the overall resistive properties of the LoG device. This is understandable when considering the values of light and dark resistance for bulk SI-GaAs, shown in Table 1. This proves that SI-GaAs is highly sensitive to 800 nm light and increases the overall photocurrent in the LoG device. For the LoQ device, however, no carriers are generated in the quartz substrate.

4.1.1.　Emission in reflection

The time-domain pulses obtained from the LoQ and LoG emitters, measured using electro-optic sampling are shown in Fig. 2. In this and all subsequent figures, the black and red curves represent the response from the LoQ and LoG devices, respectively. The applied field was set to $12.5\,kV\,cm^{-1}$ in each case and an average optical power of 500 mW was used. While using reflection geometry, the optical power and electrical bias was maintained at these values, unless otherwise stated. Under these conditions, the peak THz field measured from the LoQ device was approximately 2.6 times that obtained from the LoG device. The inset in Fig. 2 shows IV curves for each device, measured with an average optical power of 200 mW. The significantly higher photocurrent observed within the LoG device is attributed to the additional current path through the SI-GaAs substrate. The dependence of the peak-to-peak THz field on applied bias and optical power for both emitters is plotted in Fig. 3. At low applied fields, below $5\,kV\,cm^{-1}$, the response of the emitters is almost identical. This implies that in this geometry, no significant advantage is gained from the lower refractive index of the Z-cut quartz. As the field across the emitter is increased, the output signal from the LoQ device increases linearly to a maximum of $\sim1\,kV\,cm^{-1}$, achieved at an operating applied field of $40\,kV\,cm^{-1}$. This working range is limited by the breakdown field of the nitrogen purged atmosphere (approximately $35\,kV\,cm^{-1}$) [31]. In comparison, the response of the LoG emitter was sub-linear until the device suffered catastrophic failure at $13\,kV\,cm^{-1}$. At the maximum operating voltage for each device, the LoQ device emitted approximately eight times higher peak THz field than the equivalent LoG emitter. The inset in Fig. 3 shows the detected THz field plotted as a function of optical power, for an applied field of $5\,kV\,cm^{-1}$. This measurement was performed using PC detection. Again, saturation behaviour is observed in the LoG device, while the response of the LoQ device remains almost linear.

　Several conclusions have been drawn from these observations. Firstly, as the maximum field applied to the LoG device ($13\,kV\,cm^{-1}$) agrees well with the breakdown field in SI-GaAs [23], this suggests that the field that can be applied across a given electrode gap is limited by its substrate properties. Secondly, it appears that heating of the LoG device, originating from parasitic current in the SI-GaAs substrate, causes a reduction in the emitted power at a given bias
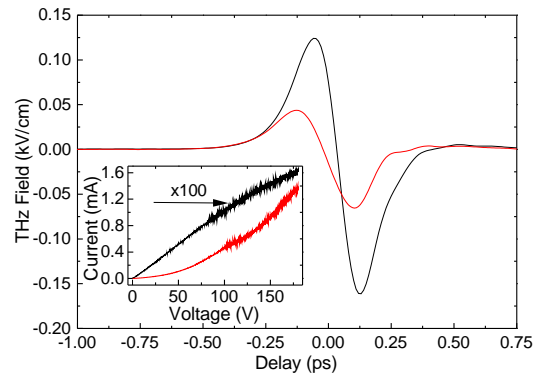
Fig. 2. (Reflection) The ultrafast terahertz time-domain pulses of LT-GaAs on quartz (LoQ) (black) and on SI-GaAs (LoG) (red). The inset shows the IV from each device measured with average optical power of 200 mW. The current for the LoQ device has been multiplied by 100.

and optical fluence. In bulk SI-GaAs, a reduction in carrier mobility and thermal conductivity with increased temperature is well documented [28,32], and is attributed to the increased probability of carriers occupying low mobility valleys higher in the conduction band [33]. Additionally, a higher phonon density results in increased scattering. We note, however, that despite LT-GaAs being a commonly used material for THz emission, a detailed analysis of its high temperature (>300 K) photoconductive emission performance is lacking. However, there is no reason to suggest that these heating effects are not a common characteristic that reduces the THz generation efficiency in LT-GaAs. It has been shown that an elevated temperature also reduces the breakdown field in LT-GaAs [23], which might also contribute to failure of the LoG device.
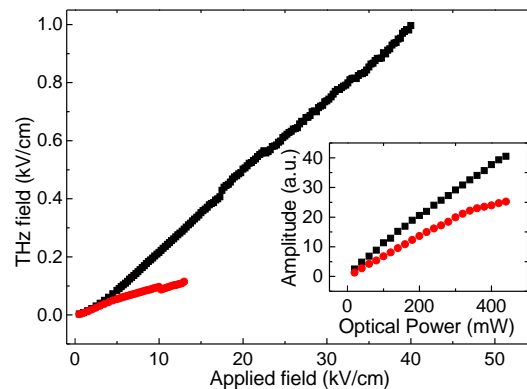

Fig. 3. (Reflection) Shows the peak-to-peak value of the THz field, extracted from the time-domain signals, as a function of applied field. The inset shows the variation of peak-to-peak output amplitude with incident optical power. In both cases, the black curve represents the LoQ device and the red curve represents the LoG device

4.1.2. Emission in transmission

We have further characterised these devices by collecting THz radiation in a transmission geometry. As discussed previously, this involves focussing the NIR beam directly onto the LT-GaAs and collecting the THz radiation from the opposite (substrate) side of the antenna. In this

instance, an identical fabrication process was followed. However, to limit the absorption of the THz signal, the LT-GaAs was transferred onto a 500-μm-thick quartz substrate. The TDS setup used for this measurement was pumped by a different mode-locked Ti:sapphire laser, providing 100-fs-wide pulses at 80 MHz repetition rate, while a 2-mm-thick ZnTe crystal was used for electro-optic detection. As can be seen in Fig. 4, this arrangement showed a similar enhancement from the LoQ device. The main figure shows the peak-to-peak THz field plotted as a function of applied bias, measured using an average optical power of 300 mW. The difference in the response of the two emitters at high applied fields ($\gtrsim 6\,\mathrm{kV\,cm^{-1}}$) is attributed to the detrimental effects of heating caused by the parasitic substrate current, previously discussed. The response at lower applied fields may be caused by a higher THz dispersion in the SI-GaAs substrate reducing the peak-to-peak field. This is inferred from the time-domain traces displayed in the inset of Fig. 4, which shows that the response from the LoG device is slightly broader, and has a larger trailing oscillation, compared with that of the LoQ emitter. These were collected using an average optical power of 300 mW and at an applied field of $10\,\mathrm{kV\,cm^{-1}}$.
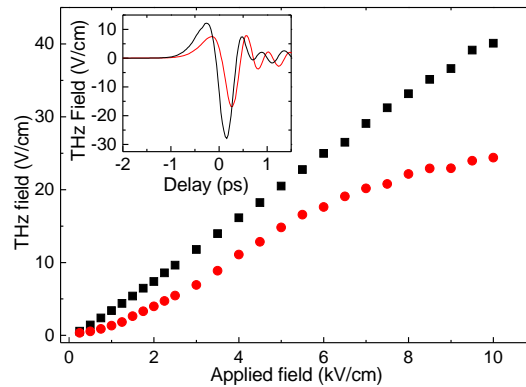

Fig. 4. (Transmission) Main figure shows the variation of peak-to-peak THz field with applied field. The inset shows time-domain pulses for both emitters under the same bias conditions. In both cases, the black curve represents the LoQ device on a 500-μm-thick quartz substrate, and the red curve is that of the LoG

4.2. Detection

In addition to PC emission, the LoQ and LoG devices were also characterised as PC detectors. The pulsed excitation laser and PC devices used here are identical to those used for the reflective THz emission measurements; the 200 μm gap is larger than would typically be used for PC detection [34] and the device geometries have not been optimised for this purpose. The detectors were positioned in the setup such that the optical beam and the THz radiation were incident on the surface of the LT-GaAs. For the detector comparison, a single LoQ emitter was used, which was biased at $5\,\mathrm{kV\,cm^{-1}}$ and illuminated with an average optical power of 500 mW, unless otherwise stated. Fig. 5(a) shows the peak-to-peak signal measured as a function of incident optical power focused onto the detector, and Fig. 5(b) shows the peak-to-peak signal as a function of bias applied to the emitter. In both instances, the peak field measured from the LoQ detector was more than twice that measured with the LoG detector. Fig. 5(c) shows the THz time-domain pulses detected from both devices. As can be seen, the LoQ detector shows a significantly larger second (negative) peak when compared with the trace from the LoG detector. This feature suggests that the SI-GaAs in the LoG device has a detrimental effect on its detection sensitivity. To explore this phenomenon, numerical simulations of the corresponding signals were performed, calculated by solving the set of coupled differential equations given in Ref [35] for the free-carrier density,

carrier velocity, and space-charge separation. We have extended these equations to account for two layers (LT-GaAs and SI-GaAs in this case):

$$\frac{dP_{sc1}}{dt} = -\frac{P_{sc1}}{\tau_{r1}} + n_{f1}ev_1 \tag{1}$$

$$\frac{dv_1}{dt} = -\frac{v_1}{\tau_{s1}} + \frac{e}{m^*}\left(E_{bias}(t) - \frac{P_{sc1} + P_{sc2}}{\eta\epsilon_0\epsilon_r}\right) \tag{2}$$

$$\frac{dn_{f1}}{dt} = -\frac{n_{f1}}{\tau_{c1}} + \alpha G(t) \tag{3}$$

$$\frac{dP_{sc2}}{dt} = -\frac{P_{sc2}}{\tau_{r2}} + n_{f2}ev_2 \tag{4}$$

$$\frac{dv_2}{dt} = -\frac{v_2}{\tau_{s2}} + \frac{e}{m^*}\left(E_{bias}(t) - \frac{P_{sc1} + P_{sc2}}{\eta\epsilon_0\epsilon_r}\right) \tag{5}$$

$$\frac{dn_{f2}}{dt} = -\frac{n_{f2}}{\tau_{c2}} + (1-\alpha)G(t) \tag{6}$$

where the subscripts '1' and '2' denote the LT-GaAs top layer and SI-GaAs/quartz substrate respectively. Here, P_{sc} is the space-charge, v is the carrier velocity, n_f is the free-carrier density, $G(t)$ is the carrier generation function from the optical pulse and α is the fraction of the optical pulse absorbed in the top layer with a factor $(1-\alpha)$ absorbed in the GaAs substrate. $E_{bias}(t)$ is the bias applied by the THz pulse. In this implementation, the space-charge effects in each layer are summed to find the reduction in effective bias across both layers; this assumption is valid since the layer thicknesses are significantly less than the antenna gap width. The parameters used in the calculation are given in Table 2.

Table 2. Parameter values used to simulate the measured signal.

Parameter	Value	Description
ϵ_r	13.1	Relative permittivity of GaAs
m^*	$0.067m_e$	Effective electron mass
η	3	Geometric factor
τ_{r1}	1 ns	Recombination time, LT-GaAs
τ_{c1}	0.4 ps	Carrier lifetime, LT-GaAs
τ_{s1}	30 fs	Momentum scattering time, LT-GaAs
τ_{r2}	1 ns	Recombination time, SI-GaAs
τ_{c2}	400 ps	Carrier lifetime, SI-GaAs
τ_{s2}	325 fs	Momentum scattering time, SI-GaAs
α	0.97	Optical pulse fraction absorbed

The generation function, $G(t)$, is given by a Gaussian pulse shape, assuming a FWHM of 20 fs, and corresponding to a power of 120 mW. For the case of a quartz substrate there is no optical absorption and the second term on the RHS of eqn. 6, $(1-\alpha)G(t)$ is set to zero. The applied bias is parameterised using the function:

$$E_{bias} = E_{THz}\sin(\omega_P(t-t_0))\text{sech}\left(\frac{1.76(t-t_0)}{t_p}\right) \tag{7}$$

Where the parameter values $E_{THz} = 0.2\,\text{kV cm}^{-1}$, $\frac{\omega_P}{2\pi} = 1$ THz and $t_p = 0.1$ ps were determined by comparison to the pulse measured in Fig. 2.

The simulation then proceeds by integrating the net transient current flowing in the PC detector at each delay time, t_0, to find the expected measured current, as shown in Fig. 5(d). Also shown
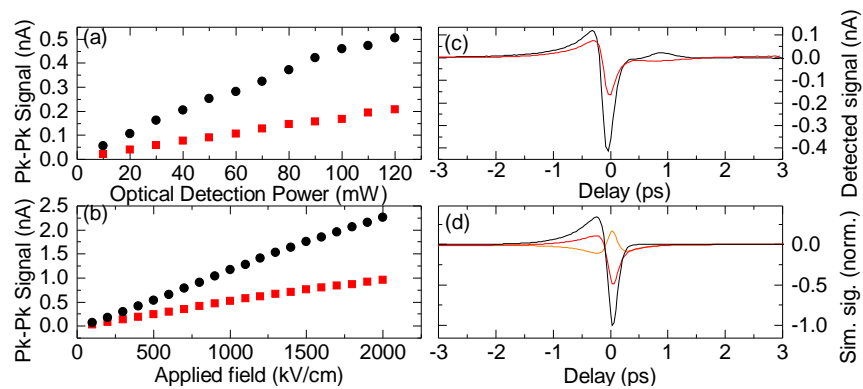
Fig. 5. Detected photo-current as a function of (a): the average optical excitation power focused on the detector and (b): the field applied to the emitter. (c): Detected time-domain signals from both devices. (d): Simulation results of time-domain traces for both detectors. The orange curve shows the contribution from the SI-GaAs substrate. In all instances, the LoQ detector is represented by the black line, while that on Si-GaAs in the red line.

in this figure is the photocurrent induced in the SI-GaAs substrate (orange curve), which has the opposite sign to the current in the LT-GaAs of the LoG detector. From this simulation we determine that the reduction in detected current measured for the LoG device relative to the LoQ device is due to space-charge effects in the SI-GaAs substrate. Due to the longer momentum scattering time (higher mobility) in the SI-GaAs, the space-charge builds up more quickly in this layer, despite the smaller optical intensity transmitted to this layer. This amounts to screening of the THz pulse, particularly the second peak, in the SI-GaAs substrate that leads to a current acting in the opposite direction to the photo-current in the LT-GaAs layer, reducing the overall measured current. Physically, the damping effect of space-charge separation in the substrate causes the substrate current to experience a phase shift. For these calculations we have also included the effect of the different substrate indexes on the reflection/transmission amplitude coefficients of the incident THz fields. This results in the THz field in the LT-GaAs layer, when on the quartz substrate, to be a factor of $(1+n_{GaAs})/(1+n_{quartz})$ higher than that for the GaAs substrate. This also acts to increase the expected current measured in the LoQ detector. Using the same parameters, these simulations also allow us to accurately recover the light resistance values for the two LT-GaAs-based-devices (LoQ and LoG), given in Table 1. The excitation intensity used in the simulation was adjusted (equivalent to adjusting the spot size/focus) to maximise signal, or photo-current, as in the experiments. Furthermore, simulations were also performed to determine the effect that carrier screening has on THz emission. However, due to the unidirectional acceleration of carriers, it was found that this contribution is minimal.

To further compare the performance of emitters and detectors under investigation in this work with the performance of a more conventional THz-TDS system, we have plotted normalised time-domain traces in Fig. 6. The red curve shows the response of the conventional TDS arrangement, employing a LoG emitter (with THz collection from the laser-excited surface) and electro-optic sampling for detection. This response shows four separate system reflections; as labelled, those occurring at 5, 10 and 17.5 ps originate from the 150-μm-thick electro-optic crystal, whereas the largest system reflection, arriving at 12.5 ps, originates from the 500-μm-thick SI-GaAs emitter substrate. The black trace shows the response when both emitter and detector are replaced with LoQ devices (with 2-mm-thick quartz substrates). In this case the first system reflection arrives 30 ps after the original pulse, originating from the interface between the air and the 2-mm-thick Z-cut quartz substrate. Owing to smaller contrast
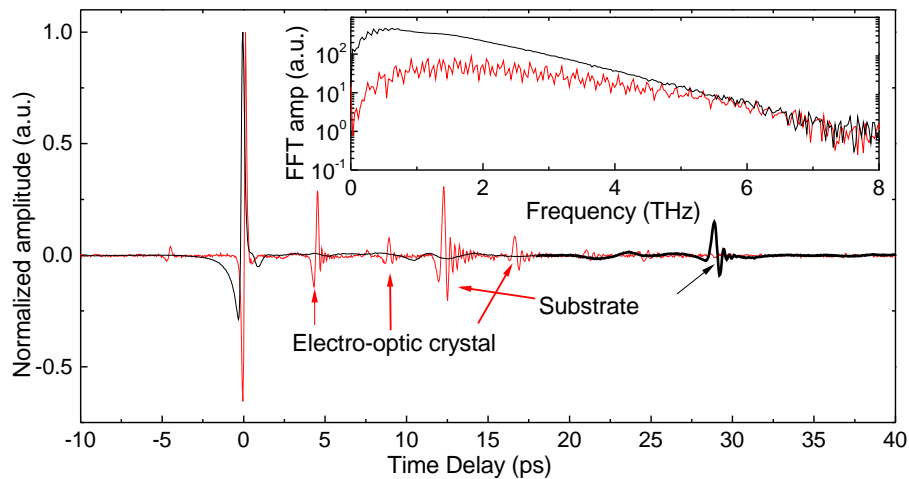
Fig. 6. Normalised time-domain trace using LoG emitter with 150-μm-thick GaP electro-optic detection crystal (red line) and LT-GaAs on a 2-mm-thick quartz substrate as emitter and detector (black line). In both instances a $5\,kV\,cm^{-1}$ bias and $500\,mW$ average optical power were applied to the emitter. Inset: FFT of the same data, normalised to the noise level and calculated with a time window of 35 ps, i.e. truncated before the quartz substrate reflection

in refractive index between quartz and air, compared to SI-GaAs and air, this reflection appears significantly smaller in the LoQ-based system. The reflection has also experienced dispersive effects, having passed twice through the quartz substrate. This reduction in system reflections increases the available frequency resolution of the system without the need for post-processing techniques [36–38]. The inset to Fig. 6 displays the corresponding fast Fourier transforms of the time-domain traces, normalised to the noise in each case. In addition to the significantly greater SNR obtained from the LoQ devices, a smoother frequency-domain response, caused by the reduction in system reflections, is also evident. In this instance, we are able to perform a scan of delay six-times longer before the first reflection is recorded, resulting in a six-fold improvement in frequency resolution. However, in principle, there is no limit to the thickness of quartz substrate that can be employed in these devices, and used in reflective-orientated emission or THz detection. It should also be noted that here both emitters have been biased with the same field/bias of $5\,kV\,cm^{-1}/100\,V$, whereas the bias of the LoQ emitter can be increased further by approximately a factor of eight.

5. Conclusion

In conclusion, epitaxial lift-off and van der Waals bonding techniques have been used to transfer LT-GaAs active layers onto quartz substrates, realising an alternative layered material combination for large-area THz photo-conductive emitters and detectors. It has been shown that these devices have three significant advantages over more widely-used PC emitters and detectors. The reduction in dark current and parasitic photo-current in quartz-based devices leads to reduced heating and increased breakdown voltages, resulting in THz field amplitudes approximately eight-times larger than those obtained from equivalent devices formed using LT-GaAs on SI-GaAs substrates. When used for PC detection the absence of an SI-GaAs substrate also eliminates the long-lifetime carriers and increases the measured signal. Furthermore, the ability to choose a thicker substrate allows system reflections to be delayed in time and their amplitude

to be reduced without a loss of bandwidth, thereby increasing the available frequency resolution.

Funding